



Development of a novel cathodic plasma/electrolytic deposition technique part 1: Production of titanium dioxide coatings

T. Paulmier^a, J.M. Bell^{a,*}, P.M. Fredericks^b

^a Faculty of Built Environment and Engineering, Queensland University of Technology, GPO Box 2434, Brisbane, QLD 4001, Australia

^b School of Physical and Chemical Science, Queensland University of Technology, GPO Box 2434, Brisbane, QLD 4001, Australia

Abstract

A new atmospheric pressure plasma electrolytic deposition process has been developed for the production of crystalline titanium dioxide films on metal substrates. The process occurs in a liquid precursor composed of titanium tetraisopropoxide and absolute ethanol. A plasma discharge is created and confined around the cathode in a superheated vapour sheath surrounded by the liquid phase, inducing the production of a nano-crystalline TiO₂ coating at the surface of the cathode. The analysis of the structure and composition of these TiO₂ coatings have been carried out by Scanning Electron Microscopy, Transmission Electron Microscopy, Raman and X-Ray Photoelectron Spectroscopies and X-Ray Diffraction. The produced crystalline titanium dioxide coatings are very adherent to the substrate and present a dendritic-like structure. We have moreover demonstrated that it is possible to adjust easily its composition by a post-processing calcination. Such characteristics make these films very interesting for photocatalysis, solar cells and gas sensing applications, and promise therefore some useful industrial benefits.

© 2006 Elsevier B.V. All rights reserved.

Keywords: Titanium dioxide films; Titanium tetraisopropoxide; Plasma electrolysis

1. Introduction

Titanium dioxide has received a great deal of attention due to its advantageous physical properties. Its high refractive index makes this material very useful for anti-reflection coating in solar cells. Its high dielectric constant, wide band-gap and high electron mobility are moreover very attractive for dye-sensitized solar cells and photo-catalysis applications [1–3]. This material can also be used in gas sensor technology [4,5].

Titanium dioxide coatings can be produced using various methods such as sol-gel coating [6–8], thermal CVD [9–11] and plasma enhanced CVD (PECVD) [12,13]. Titanium tetraisopropoxide has been used very often as a precursor in the vapor state for TiO₂ coating. Most of these deposition processes are carried out at low pressure, requiring sometimes an oxygen source, and making therefore these methods quite expensive. Moreover the treatment time of these processes can reach several hours, further increasing the production cost of the coating.

A new cathodic plasma electrolytic deposition method has been developed allowing, at atmospheric pressure and in a few

minutes, the production of nano-structured TiO₂ films with excellent adhesion. This process combines galvanic processes and plasma-chemical phenomena. Unlike other plasma deposition techniques, the process occurs in liquid precursors and the plasma is confined to the cathode in a superheated vapour sheath surrounded by the liquid phase.

In the current paper, we have investigated the structure, morphology and composition of the titanium dioxide coatings by Secondary Electron Microscopy (SEM), X-Ray diffraction (XRD), Raman spectroscopy, X-Ray Photoelectron Spectroscopy (XPS) and Transmission Electron Microscopy (TEM). These characteristics have been studied as a function of the treatment time and injected electric power. The TiO₂ coatings have been submitted to a post-treatment annealing process in order to study the evolution of the composition and crystallinity of the coatings with the calcination temperature.

2. The experimental set-up

The basic principle of the plasma electrolytic deposition system is to apply a high voltage between two electrodes immersed in a liquid electrolytic solution. The surface area of the cathode being much lower than that of the anode ($A_{\text{cathode}}/A_{\text{anode}} \approx 0.08$), the

* Corresponding author. Tel.: +61 7 3864 4298; fax: +61 7 3864 1529.

E-mail address: j.bell@qut.edu.au (J.M. Bell).

electric field is higher near the cathode inducing a strong Joule heating in the vicinity of this electrode which triggers the formation of a vapour sheath around the cathode. As the electric conductivity of this vapour sheath is much lower than the electric conductivity of the liquid solution, the voltage drop occurs primarily within the vapour sheath, inducing a strong electric field within the separated bubbles. If the applied voltage is sufficiently high, the electric field within the bubbles will cause the electrical breakdown of the gas and the initiation of a plasma glow discharge within the bubble. As the voltage increases the plasma discharge stretches all along the surface to cover the entire cathode at a given voltage depending on the composition and electric resistance of the solution. The physical characteristics of the plasma discharge are presented in reference [14]. These glow discharges induce the dissociation of the vaporised electrolyte and the formation of a continuous coating on the cathode.

The plasma electrolytic reactor is composed of a jacketed glass vessel with an inner volume of 1 dm³ (Fig. 1). This vessel is cooled by a water flow in order to control and adjust the temperature of the liquid solution. A set of electrodes is maintained within the

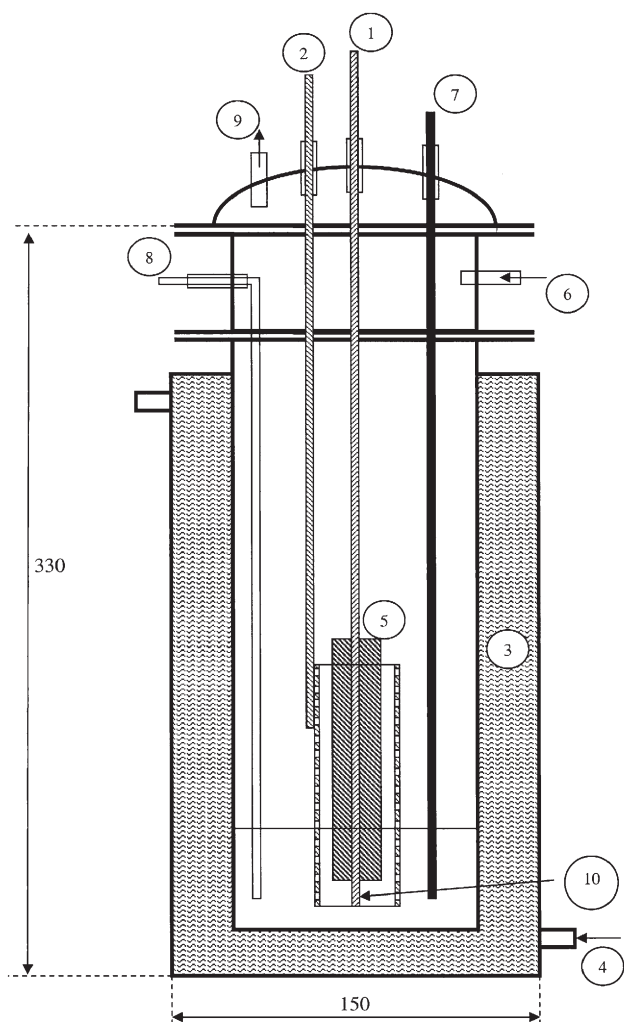


Fig. 1. Scheme of the plasma reactor. 1: Cathode support, 2: Anode, 3: Jacketed glass vessel, 4: Water inlet, 5: Teflon shield, 6: Solution addition, 7: Thermometer, 8: Solution sampling system, 9: Gas exhaust, 10: Treated Cathode.

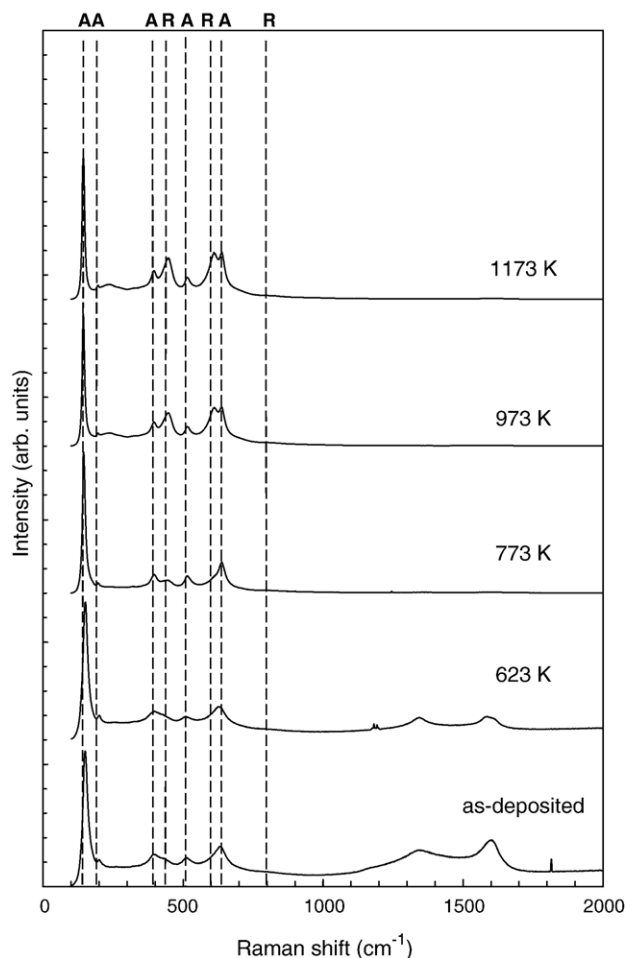


Fig. 2. Raman spectra of the titanium dioxide coatings produced at 1000 V for 300 s with a solution composed of TTIP (40%), ethanol (58.8%) and HCl (0.2%), as-deposited and calcinated at 623 K, 773 K, 973 K and 1173 K (A: Anatase, R: Rutile).

liquid solution by two copper and stainless steel supports which also allow connection to the electrical power supply. The length of the centred cathode is adjusted at 10 mm using a 100 mm long PTFE shield. The cathode is a 3.1 mm diameter Cu metallic rod. The surrounding anode is a 40 mm inner diameter cylinder composed of graphite to avoid any oxidation of the anode and any metallic deposition of anodic element on the cathode. This plasma reactor operates at 10⁵ Pa and is blanketed by a continuous flow of nitrogen to avoid any flames or explosion within the glass vessel. The reactor is powered by a DC power supply (Bertran 105-02R) with a maximum voltage of 2000 V, a maximum power output of 1 kW and a maximum current of 500 mA.

Titanium tetraisopropoxide (TTIP, Ti(OC₃H₇)₄, Sigma–Aldrich, 97%) was used as precursor for the production of TiO₂ films. The TTIP solution was distilled and stored under nitrogen. 100 cm³ of TTIP was added to 150 cm³ of absolute ethanol and 0.1 to 1.5 cm³ of hydrochloric acid (HCl) (concentration: 31.5% w/w). The function of hydrochloric acid is mainly to adjust the electric current in the liquid phase. The cathode was treated in the plasma reactor for 30 to 300 s at a maximum voltage varying from 650 to 1200 V, depending on the liquid composition. The current density during the plasma treatment is around 330 mA cm⁻². The

resulting TiO₂ coatings were annealed at atmospheric pressure in air for 1 day at 623 K, 773 K, 973 K or 1173 K.

3. The analytical tools

The composition and crystallinity of the TiO₂ samples were studied by XRD, Raman spectroscopy, TEM and XPS. Visible Raman spectra were measured using a Renishaw InVia Raman microprobe spectrometer equipped with laser excitation at 532 nm (20 mW at the sample) and a 50× microscope objective. X-ray diffraction patterns were collected using a Philips X'pert wide angle X-ray diffractometer, operating in step scan mode, with Cu K α radiation (1.54052 Å). Patterns were collected in

the range 3–90° 2 θ with a step size of 0.02° and a rate of 30 s/step. The samples were scanned using an X-ray beam at a grazing incidence of 1°.

The crystallite size L in the coatings can be determined from the full width at half maximum β of the corresponding peaks, using Sherrer's formula [15]:

$$L = \frac{K \cdot \lambda}{\beta \cdot \cos \theta} \quad (1)$$

where λ is the wavelength of the X-ray radiation, K is a constant value taken as a default value of 0.89, and θ the X-ray diffraction angle of the corresponding peak.

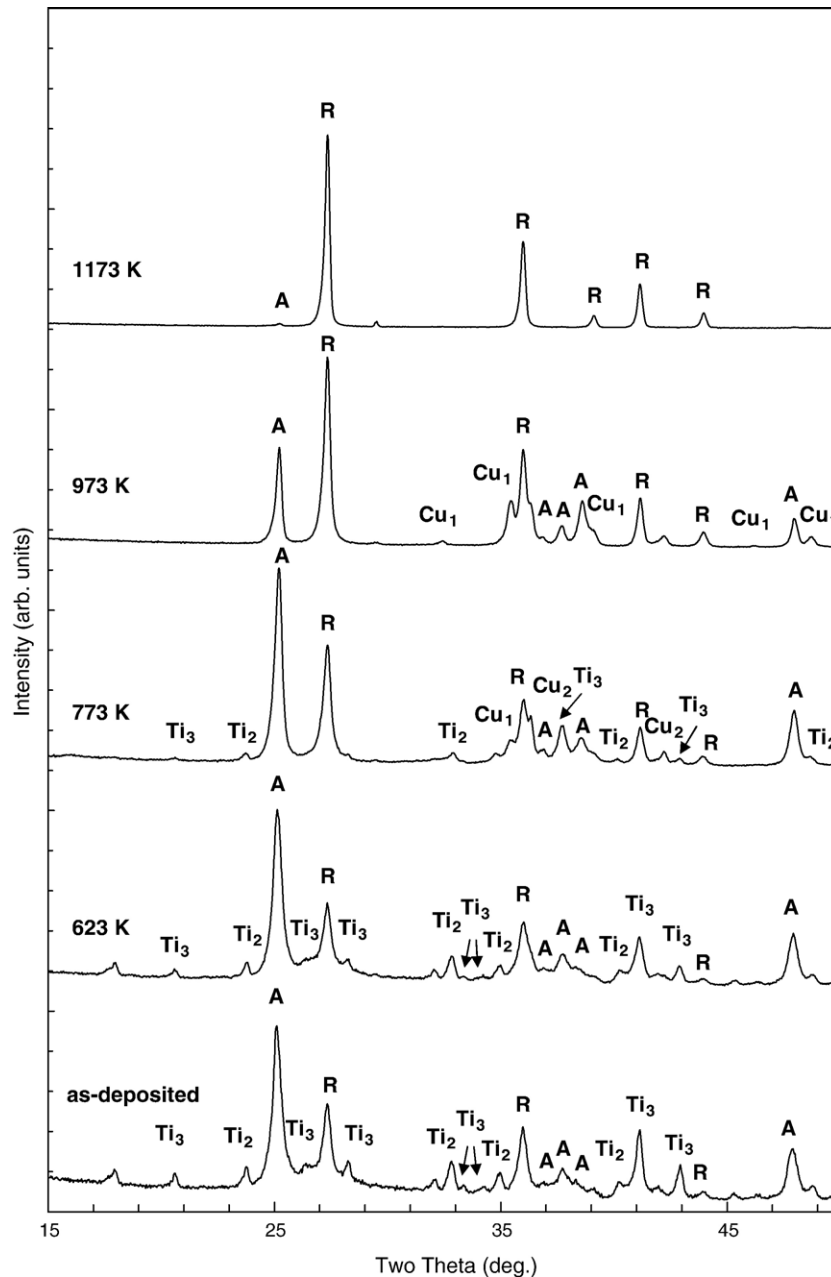


Fig. 3. X-Ray diffraction spectra of the titanium dioxide coatings produced at 1000 V for 300 s with a solution composed of TTIP (40%), ethanol (58.8%) and HCl (0.2%), as-deposited and calcinated at 623 K, 773 K, 973 K and 1173 K (A: Anatase, R: Rutile, Ti₂: Ti₂O₃, Ti₃: Ti₃O₅, Cu₁: CuO, Cu₂: Cu₂O).

Table 1
Rutile content in the TiO₂ phase and crystallite size (anatase and rutile) for the as-deposited and calcinated titanium dioxide coatings

Samples	Rutile/ (rutile+anatase) %	Crystallite size (nm)	
		Anatase	Rutile
As-deposited	38	30	39
Calcinated	623 K	27	23.5
	773 K	36.5	42.5
	973 K	57	51.5
	1173 K	–	82

The rutile to (rutile + anatase) ratio can be calculated from the intensities of the anatase and rutile peaks, by the relation [15]:

$$x = \left(1 - 0.8 \frac{I_A}{I_R}\right)^{-1} \quad (2)$$

where x is the weight fraction of rutile, and I_A and I_R the integrated X-ray intensities of the (101) reflection peak of anatase at $2\theta=25.4^\circ$ and the (110) reflection peak of rutile at $2\theta=27.5^\circ$.

TEM pictures were obtained with a Phillips CM200 TEM operated at 200 kV. In this case, the films were removed from the substrate and deposited in an ethanol suspension on a carbon film coated grid. XPS data were acquired using a Kratos Axis ULTRA X-ray Photoelectron Spectrometer incorporating a 165 mm hemispherical electron energy analyser. The incident radiation was Monochromatic Al X-rays (1486.6 eV) at 150 W (15 kV, 10 mA). Survey (wide) scans were taken at an analyser pass energy of 160 eV and multiplex (narrow) high resolution scans at 20 eV. The morphology of the TiO₂ coatings has been studied by SEM using a FEI Quanta 200 Environmental SEM. Surface analysis was carried out on the films without further preparation.

4. Experimental results

4.1. Film structure and composition

The coatings presented in this section have been produced using a solution of TTIP (40% vol.), ethanol (58.8% vol.) and HCl (0.2% vol.) which was treated for 300 s at 1000 V (ramp rate: 50 V s⁻¹). In this configuration, the average current density is equal to 330 mA cm⁻².

The structure and composition of the deposited films have been analysed by Raman spectroscopy, XRD, XPS and TEM. The analysis by Raman spectroscopy reveals that the as-deposited coating is composed of a mixture of anatase and rutile (TiO₂) and graphitic carbon (Fig. 2). This coating exhibits 5 Raman peaks at 152, 199, 390, 504 and 626 cm⁻¹, corresponding to the anatase vibration modes: E_g, E_g, B_{1g}, A_{1g}+B_{1g} and E_g [16–18]. Two shoulders present at 420 and 803 cm⁻¹ correspond to the E_g and B_{1g} modes of the rutile phase, respectively. Two other peaks located at 1327 and 1598 cm⁻¹ are attributed to graphitic carbon. Carbon can come from the propyl groups of the TTIP or from the ethanol solvent. For an annealing temperature above 623 K, we can see, from the development of 3 other peaks at around 442, 607 and 803 cm⁻¹ that anatase is gradually converted into rutile. These three last peaks correspond indeed to the vibrational modes of rutile: E_g, A_{1g} and B_{1g} [16–18]. A small broad multiple peak at 230 cm⁻¹, especially conspicuous above 773 K, is due to a second order process in rutile vibrational modes [19]. We can moreover notice that the Raman intensity of graphitic carbon decreases significantly once the coating is submitted to a calcination process. The carbon phase present initially in the coating is therefore rapidly oxidised by the thermal treatment in air. The fact that titanium dioxide is in the form of anatase and rutile in the films indicates that these oxide coatings have been produced during the process by the plasma discharge and not by oxidation in air after the plasma treatment which would lead to an amorphous titanium

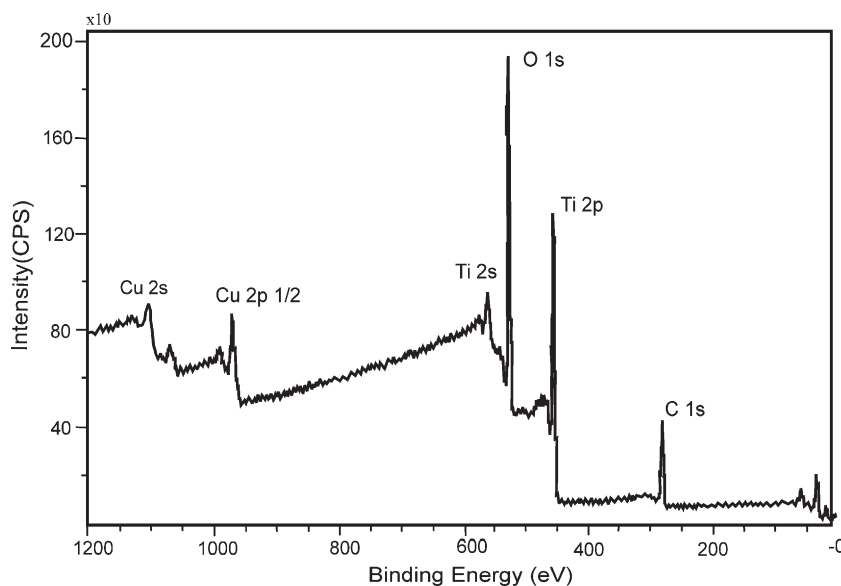


Fig. 4. Full XPS spectrum of the as-deposited TiO₂ coating.

dioxide coating. In our case, the only high temperature source is the plasma discharge. Titanium dioxide is therefore produced within the plasma discharge, converted in anatase and rutile and deposited at the surface of the cathode.

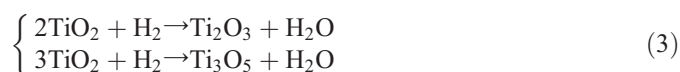
The X-Ray diffraction reveals a more complicated composition. As we can see in Fig. 3, the crystalline phase of the as-deposited coating is composed of anatase, rutile, Ti_2O_3 and Ti_3O_5 . These two last by-products are certainly the result of the reduction at the vicinity of the cathode of TiO_2 formed in the gas phase by the plasma discharge. This reduction can be activated by some reactive organic radicals that may have a greater

Table 2

Evolution of the relative molecular concentration of TiO_2 and C for each sample, evaluated by XPS

	As-deposited	Annealed			
		623 K	773 K	973 K	1173 K
TiO_2 (%)	83	83.6	91.6	93.1	93
C (%)	17	16.4	8.4	6.9	7

affinity for oxygen than TiO_2 . It can also be explained by the reaction of TiO_2 with hydrogen produced close to the cathode [20,21]:



In the calcinated coatings (Fig. 3), we observed that Ti_2O_3 and Ti_3O_5 gradually vanish, converted to anatase or rutile phases. Ti_3O_5 and Ti_2O_3 are indeed only stable in the respective temperature ranges 473–603 K and 473–673 K. For temperatures above 773 K, the titanium dioxide is then only composed of anatase and rutile phases. We can observe, as well, the presence of CuO and Cu_2O phases in the calcinated films, coming from the oxidation of the copper substrate.

Table 1 shows the evolution of the crystallite size calculated with the Sherrer's formula for anatase and rutile and the rutile to (rutile+anatase) ratio, calculated with relation (2), in the as-deposited and calcinated coatings. The as-deposited coating is composed of 38% of rutile phase in respect to (rutile+anatase) fraction of the coating which demonstrates that the temperature of the plasma discharge is high enough to convert a significant

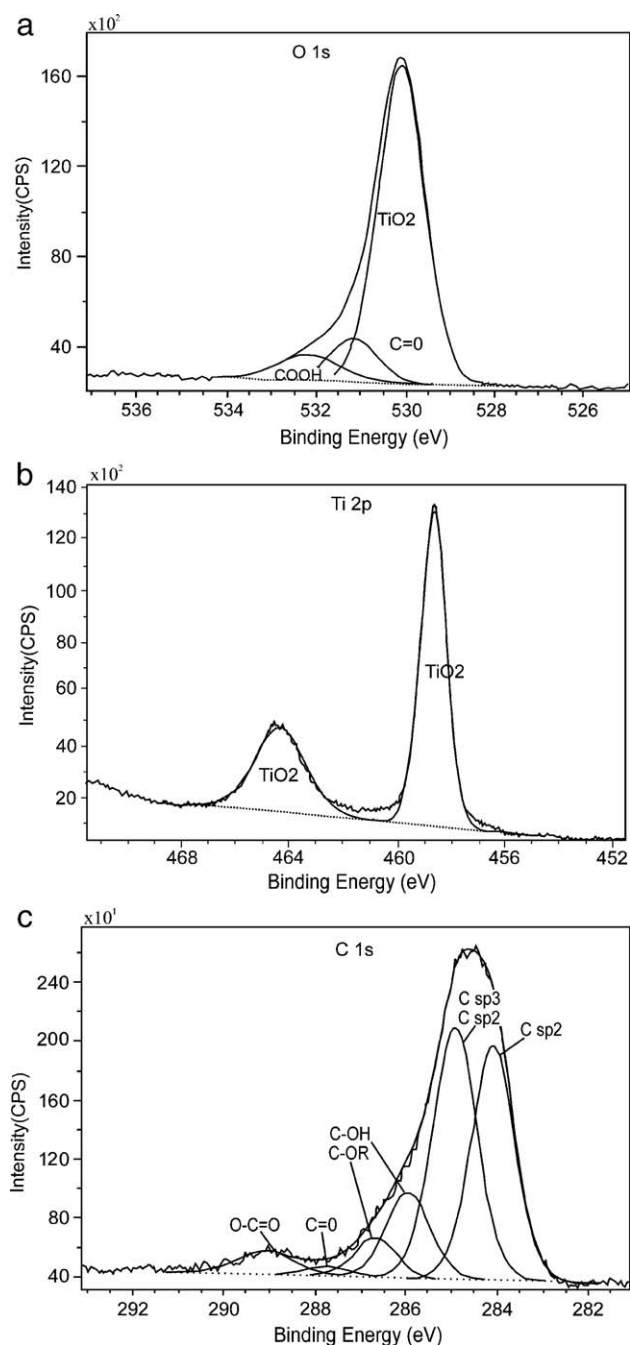


Fig. 5. High resolution analysis for the as-deposited coating of: (a) O 1s peak, (b) Ti 2p peak and (c) C 1s peak.

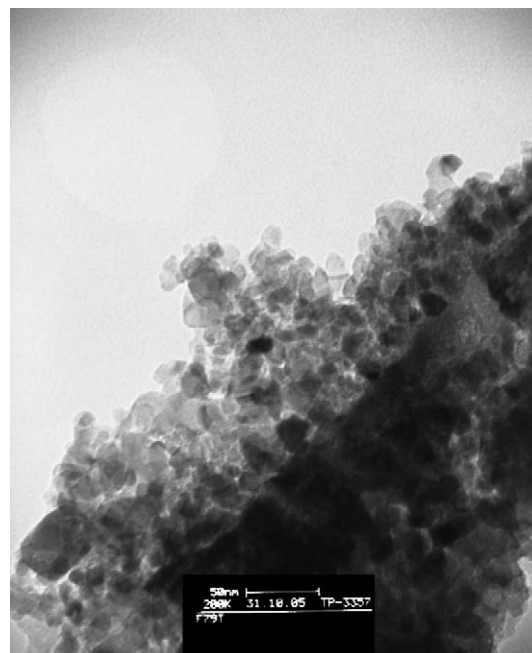


Fig. 6. TEM picture of the titanium dioxide coatings produced at 1000 V for 300 s with a solution composed of TTIP (40%), ethanol (58.8%) and HCl (0.2%) and calcinated at 623 K.

proportion of anatase to rutile. As we increase the temperature above 623 K, anatase is rapidly converted to rutile, leading to a coating composed of 99% of rutile in TiO_2 phase at 1173 K. From these measurements, we can deduce that the plasma temperature is lower than 773 K. Otherwise the post-heat treatment should not have a significant effect on the structure of the coating.

The average crystallite size of the anatase and rutile phases in the as-deposited films is respectively 30 and 39 nm. It increases significantly after the annealing treatment above 623 K to reach 82 nm at 1173 K for the rutile coating. We can notice a decrease of the crystallite size between the as-deposited coating and the film calcinated at 623 K. This may be explained by the fact that a rearrangement of titanium and oxygen atoms within the anatase phase occurs at this temperature level. Rutile nucleation and growth from anatase grain requires a minimum breaking of Ti–O bonds. At 623 K, we could be in an intermediate state where this breaking process leads to a decrease of the crystalline phase. The transformation involves an overall contraction or shrinking of the oxygen structure which can induce a decrease of the grains. Rutile is still quite unstable at this level which can explain the slight decrease (5%) of rutile ratio observed at 623 K. Peak broadening associated with the nucleation of rutile phase within the anatase grain could also explain the underestimation of rutile content at 623 K. As we will see further in the SEM analysis, the TiO_2 coatings are very dense: the treatment at higher temperature tends then to trigger the fusion of adjacent crystallites, increasing consequently the size of the crystallites above 623 K.

The XPS measurements show that all the samples are composed of Ti, O and C. Fig. 4 presents the full XPS spectrum for the as-deposited sample. The four main peaks easily identified at 530 eV (FWHM: 1.17 eV), 464.3 eV (FWHM: 2.21 eV), 458.7 eV (FWHM: 1.12 eV) and 283 eV (FWHM: 2.15 eV) corresponds respectively to the electronic band O 1s, Ti 2p_{1/2}, Ti 2p_{3/2} and C 1s. The shape of the Ti 2p is similar for the as-deposited and annealed samples and is assigned to Ti^{4+} 2p_{1/2} and 2p_{3/2}, bonded to oxygen in a titanium dioxide phase [22,23]. The XPS spectra have then been realigned using the theoretical position of Ti 2p_{1/2} in TiO_2 at 458.7 eV to take into account the possible charging effect and get the real binding energies. The charging effect has been calculated from this peak: it is equal to 2.1 eV in the three different analysed films. Fig. 5 presents the high resolution deconvoluted peaks for Ti 2p, O 1s and C 1s. Titanium is therefore present in the coating mainly in the form of titanium dioxide, even in the as-deposited film. Moreover, the position of the O 1s peak at 530 eV can be assigned to TiO_2 phase. We can as well identify some oxygen bonded to carbon by the presence of another O 1s peak located at 531.1 eV (FWHM: 1.21 eV). This peak has been assigned to carbonyl group (C=O) [24]. A third peak located at 532.2 eV (FWHM: 1.6 eV) can be attributed to carboxyl groups (O–C=O) [25]. The observation can be completed by the deconvolution of the C 1s peak into 6 main peaks, located at 284.1 eV, 285.2 eV, 286 eV, 287 eV, 288 eV, 289.5 eV, which can be assigned respectively to graphite at 284.1 eV [26–29], disordered graphite or hybridized sp³ carbon at 285.2 eV [26–29], hydroxyl group (C–OH), ether

group (C–OR) or polymer-like carbon at 286 and 287 eV [27,28,30,31], carbonyl groups (C=O) at 288 eV [27,28,30,31] and carboxyl groups (O–C=O) at 289.5 eV

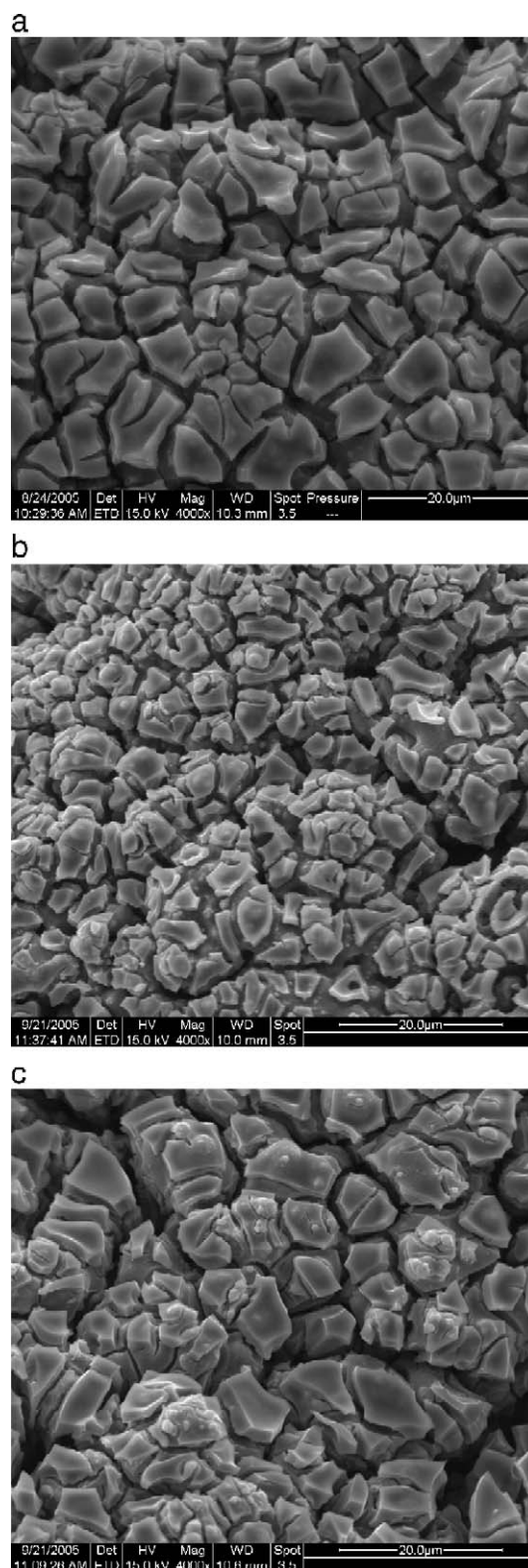


Fig. 7. SEM picture (magnification: $\times 4000$) of the titanium dioxide coatings produced at 1000 V for 300 s with a solution composed of TTIP (40%), ethanol (58.8%) and HCl (0.2%). (a) as-deposited, (b) calcinated at 623 K, (c) calcinated at 973 K.

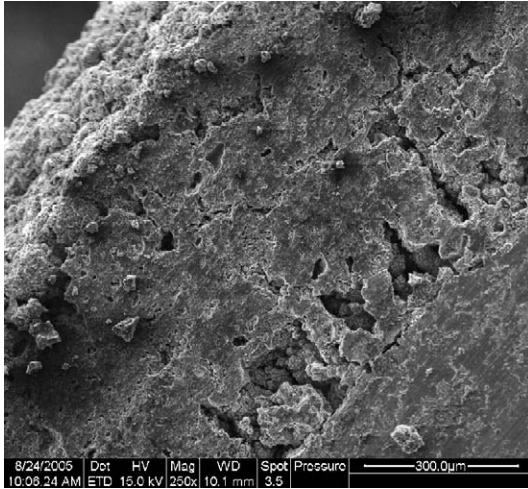


Fig. 8. SEM picture of the cross section of the as-deposited titanium dioxide coating produced at 1000 V for 300 s with a solution composed of TTIP (40%), ethanol (58.8%) and HCl (0.2%).

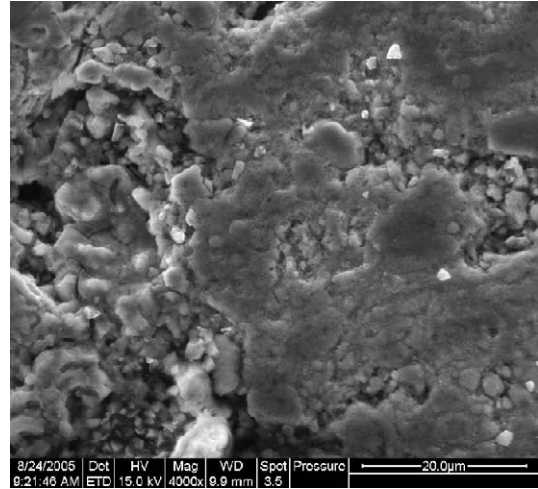


Fig. 9. SEM picture at high magnification ($\times 4000$) of the cross section of titanium dioxide coating produced at 1000 V for 300 s with a solution composed of TTIP (40%), ethanol (58.8%) and HCl (0.2%).

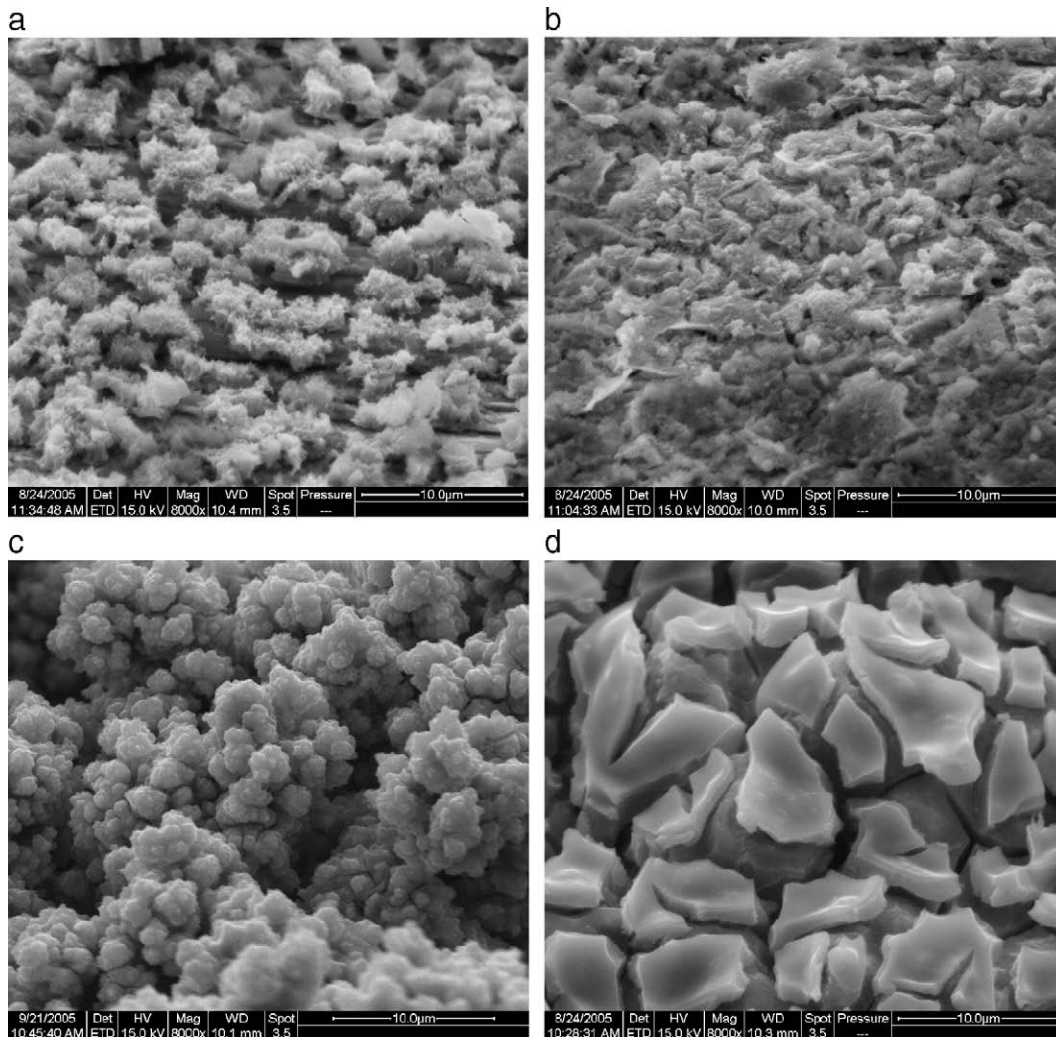


Fig. 10. SEM pictures of the titanium dioxide coatings produced at 1000 V with a solution composed of TTIP (40%), ethanol (58.8%) and HCl (0.2%) for : (a) 30'', (b) 60'', (c) 120'', and (d) 300''.

[27,28,30,31]. These peaks have been observed in all samples. They have already been detected in a previous study [32] and are due to the dissociation of ethanol by the plasma electrolytic discharge. No peak from carbon bonded to titanium, usually

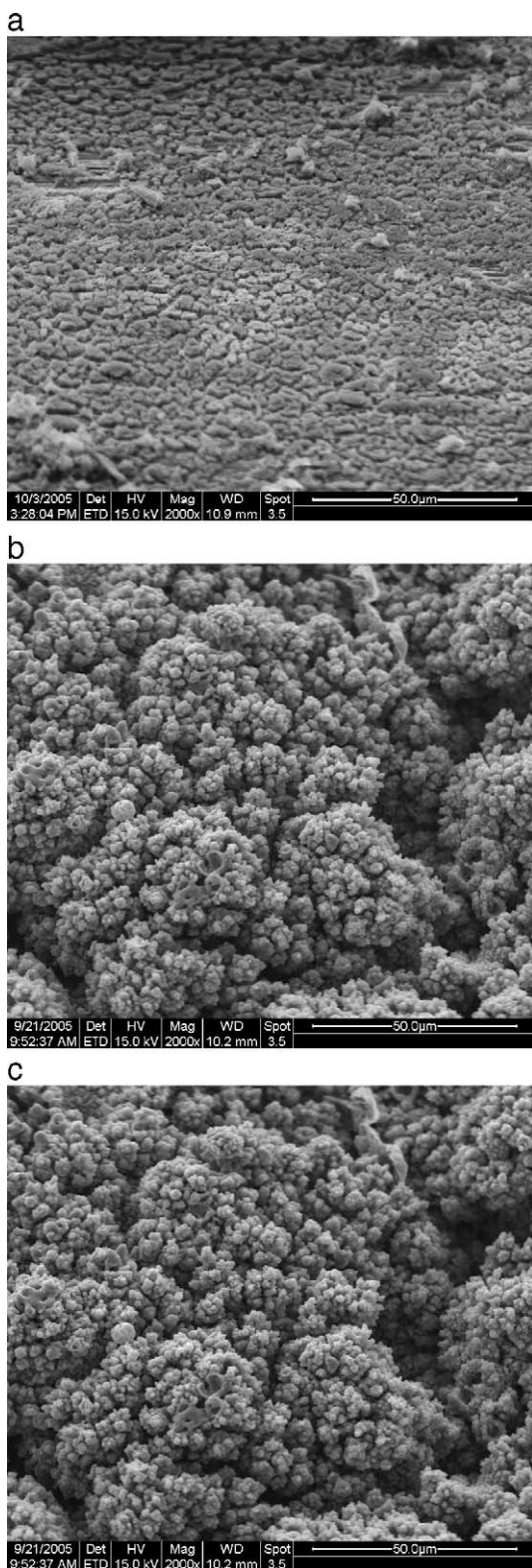


Fig. 11. SEM pictures ($\times 2000$) of the as-deposited titanium dioxide coatings produced at: (a) 218 W, (b) 274 W and (c) 338 W.

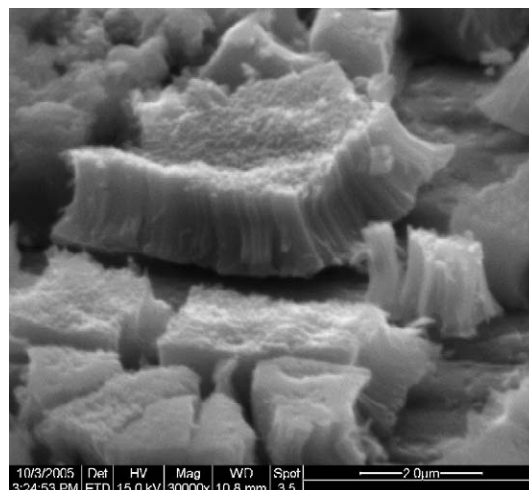


Fig. 12. High magnification ($\times 30,000$) SEM picture of the coating produced at 218 W.

present at 281.8 eV (titanium carbide TiC) and 282.6 eV (titanium subcarbide) [24,26] have been detected.

From the areas of the different XPS peaks, we have been able to evaluate the relative concentration of TiO₂ and carbon in each sample. The results are summarised in Table 2. We can then notice that the carbon concentration decreases gradually when the post-treatment temperature increases, up to 7% at 973 and 1173 K.

The samples, removed from their substrate, have been analysed as powders by TEM. The pictures reveal that the coatings are composed of TiO₂ crystalline nano-particles. Fig. 6 presents the TEM picture for the sample calcinated at 623 K. The particle size ranges from 3 nm to 30 nm, with an average of approximately 25 nm which is in a good agreement with the calculation carried out by X-Ray diffraction. We have noticed by TEM analysis that the films are very dense. The form of the nano-particles is similar to the shape of grains produced by epitaxy. The films are therefore

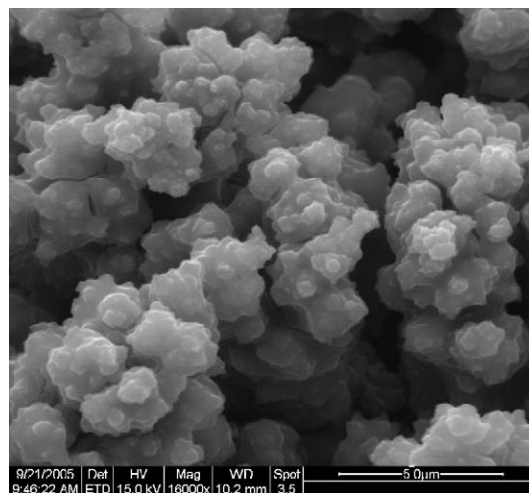


Fig. 13. High magnification ($\times 16,000$) SEM picture of the coating produced at 274 W.

made by the build-up and fusion of numerous crystallites with different size and shape.

4.2. Microstructure of the films

The characterisation of the TiO₂ coatings by SEM shows a surface presenting a large specific area with a large quantity of entangled grooves and cavities. Fig. 7 presents the morphology of the as-deposited film and the film treated at 623 K and 973 K. These films present a high open porosity and their morphology is not strongly altered by the heat treatment. As seen from the cross-section of the as-deposited sample (Fig. 8), the thickness of TiO₂ coating deposited for 300 s at 1000 V with a solution composed of TTIP (40%), ethanol (58.8%) and HCl (0.2%) is around 700 μm. The deposition rate in this case is therefore very large, equal to 2.3 μm s⁻¹. These coating have a large distribution of closed micro-pores whose diameter varies from 5 to 100 μm. The observation of the cross section at high magnification (Fig. 9) clearly shows, as deduced from the TEM measurements, that the films are the results of the fusion and accumulation of nano-crystallites at the surface of the substrate.

4.3. Influence of the operating parameters

In order to understand more thoroughly the deposition mechanisms, we have studied the influence of the treatment time, the electric power injected in the system and the applied voltage on the micro-structure of the films. Fig. 10 shows the morphology of coatings deposited with the solution described above at 1000 V for 30, 60, 120 and 300 s. The morphology is drastically altered with the treatment time. For duration lower than 120 s, the coatings are inhomogeneous, with the presence of lot of cracks through which we can see the copper substrate. At 120 s, the micro-structure of the titania coating is typical of a dendritic-like structure. The coating is composed of a build-up of micro-particles, i.e. a cluster of nano-crystallites, inducing a

highly porous structure. This structure presents therefore a high specific surface area, larger than the coating produced after 300 s.

The influence of injected electric power on the structure and morphology of the films has also been studied by varying the electric resistance of the liquid solution. This resistance has been adjusted by the concentration of hydrochloric acid present in the solution. This concentration ranges from 0.2% to 0.6% in volume: these changes have basically no effect on the chemistry of the solution but will affect significantly the resistance of the liquid solution. As the liquid phase acts as a resistive element in the plasma system, adjusting the resistance of the precursor allows the control of the power delivered to the system (liquid phase+gas phase). In these experiments, we have adjusted the voltage, for each HCl concentration, to keep up a density equal to 330 mA cm⁻². We have then worked at three different injected powers: 218 W, 274 W and 338 W. The coatings have been deposited for 300 s. Fig. 11a, b and c present the morphology of the as-deposited coatings produced at these three different powers. The micro-structure of these three coatings is drastically different: the films get denser, thicker and more homogeneous with the increasing discharge power. At 218 W, the coating is inhomogeneous with the presence of numerous cracks through which the substrate is visible (Fig. 12). This film seems to present a columnar structure noticeable through the cross section of the sample in Fig. 12. At 274 W, the coating presents a dendritic micro-structure with much larger porosity and surface area than the deposit produced at 338 W. The observation at high magnification of this film (Fig. 13) clearly reveals that it is composed of nano-crystallites melted together.

Fig. 14 presents the Raman spectra of the as-deposited coatings produced at 218, 274 and 338 W. We can then notice that the three samples are composed of anatase TiO₂. A small amount of rutile is also observed in the three samples through the shoulders present at around 230, 442 and 607 cm⁻¹.

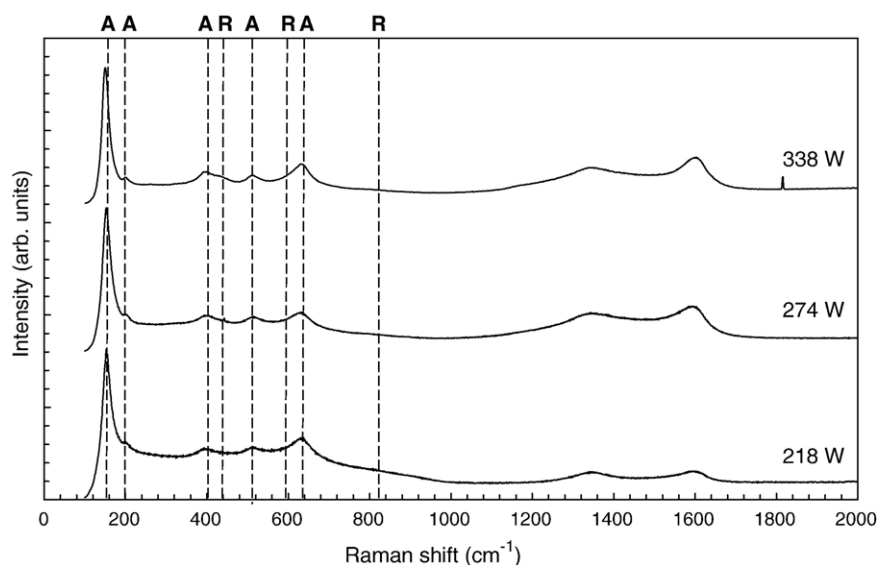


Fig. 14. Raman spectra of the as-deposited titanium dioxide coatings produced at 218 W, 274 W and 338 W.

The injected power has therefore a significant influence on the morphology of the deposited coatings. Increasing the power must enhance the power injected in the discharge itself. As we raise the discharge power, we enhance the energy gained by electrons and ions within the plasma. This energy is then transferred to atoms and molecules of the surrounding gas, leading then to an increase of the dissociation and nucleation rate and of the surface mobility of the adsorbed species. We get then much thicker and denser coating with the power rise. The difference in density is especially seen between the films deposited at 274 and 338 W. However, the temperature is not increased significantly since, in the three tests, the anatase/rutile ratio keeps up the same level. We are then able to modify the microstructure of the coating without changing drastically their phase composition.

5. Conclusion

The newly developed cathodic plasma electrolytic deposition process allows the rapid production at atmospheric pressure of thick, continuous and adherent titanium dioxide films. These coatings are mainly composed of nano-crystallites of anatase, rutile and graphitic carbon and present a complex microstructure which varies drastically with the treatment time and the electric power injected in the system. Lower titanium oxides, such as Ti_2O_3 and Ti_3O_5 , are present as well in the as-deposited coating. They can easily be entirely converted to anatase and rutile phases by annealing the samples in air at temperature higher than 773 K. The micro-structure of the deposited coating is dendritic in nature and results from the build-up of nano-crystallites of titanium dioxide produced from the dissociation of titanium tetraisopropoxide by the plasma discharge and deposited at the surface of the cathode. We have been able in this study to demonstrate that this process is very flexible allowing the production of different structures by varying the operating parameters. The initiation of the plasma discharge is essential for the deposition of titanium dioxide film. No TiO_2 deposits have indeed been observed in the absence of the plasma discharge. Its function is to decompose the vaporised solution into TiO_2 particles and to create the high temperatures needed to convert the deposited coating into a crystalline adherent one. A post-treatment calcination between 773 and 1173 K enables adjustment of the crystallite size and the relative concentrations of rutile and anatase. This thermal treatment is moreover very useful to oxidise the carbon phase initially present in the as-deposited film.

The physical characteristics of these titanium dioxide coatings (anatase/rutile composition, large surface area, good adherence) make these films very interesting for possible application in photocatalysis, solar cells or gas sensing. Due to the high deposition kinetics and the operation at atmospheric pressure without any extra supply of oxygen, this plasma process is very cheap compared with other conventional deposition techniques and is therefore very promising industrially.

Coupled with the characterisation results carried out on the TiO_2 coatings, a further comprehensive analysis on the plasma discharge, the liquid and gas phases is however necessary to get a clear knowledge on the dissociation and deposition mechan-

isms leading to the formation of a titanium dioxide film on the cathode. We will then be able to build a reaction model and control more easily the properties of the deposited coatings.

Acknowledgement

Support for this project from the Australian Research Council Discovery Grant DP0345956 is gratefully acknowledged.

References

- [1] A. Fujishima, T.N. Rao, D.A. Tryk, J. Photochem. Photobiol., C. Photochem. Rev. 1 (2000) 1.
- [2] O. Carp, C.L. Huisman, A. Reller, Prog. Solid State Chem. 32 (2004) 33.
- [3] A. Mills, S. Le Hunte, J. Photochem. Photobiol., A Chem. 108 (1997) 1.
- [4] K. Zakrzewska, Thin Solid Films 391 (2001) 229.
- [5] K. Zakrzewska, Vacuum 74 (2004) 335.
- [6] L. Miao, S. Tanemura, S. Toh, K. Kaneko, M. Tanemura, J. Cryst. Growth 264 (2004) 246.
- [7] Y.-F. Chen, C.-Y. Lee, M.-Y. Yeng, H.T. Chiu, Mater. Chem. Phys. 81 (2003) 39.
- [8] Z.-Y. Yuan, B.-L. Su, Colloids Surf., A Physicochem. Eng. Asp. 241 (2004) 173.
- [9] U. Backman, A. Auvinen, J.K. Jokiniemi, Surf. Coat. Technol. 192 (2005) 81.
- [10] K.-H. Ahn, Y.-B. Park, D.-W. Park, Surf. Coat. Technol. 171 (2003) 198.
- [11] C.P. Fictorie, J.F. Evans, W.L. Gladfelter, J. Vac. Sci. Technol., A, Vac. Surf. Films 12 (1994) 1108.
- [12] G.A. Battiston, R. Gerbasi, A. Gregori, M. Porchia, S. Cattarin, G.A. Rizzi, Thin Solid Films 371 (2000) 126.
- [13] M. Nakamura, D. Korzec, T. Aoki, J. Engemann, Y. Hatanaka, Appl. Surf. Sci. 175–176 (2001) 697.
- [14] T. Paulmier, J.M. Bell, P.M. Fredericks, Physical characteristics of the glow discharge and analysis of the vapour sheath structure in a cathodic plasma electrolytic deposition system, submitted to Surf. Coat. Technol.
- [15] A.H.C. Chan, J.F. Porter, J.P. Barford, C.K. Chan, J. Mater. Res. 17 (2002) 1758.
- [16] V.V. Yakovlev, G. Scarel, C.R. Aita, S. Mochizuki, Appl. Phys. Lett. 76 (2000) 1107.
- [17] M. Ocaña, J.V. Garcia-Ramos, C.J. Serna, J. Am. Ceram. Soc. 75 (1992) 2010.
- [18] W.-X. Xu, S. Zhu, X.-C. Fu, Q. Chen, Appl. Surf. Sci. 148 (1999) 253.
- [19] T.D. Robert, L.D. Laude, V.M. Geskin, R. Lazzaroni, R. Gouttebaron, Thin Solid Films 440 (2003) 268.
- [20] M. Codell, Analytical chemistry of titanium metals and compounds, Interscience Publishers Inc., New York, 1959.
- [21] R.J.H. Clark, D.C. Bradley, P. Thornton, The chemistry of titanium, zirconium and hafnium, Pergamon Press, Oxford UK, 1973.
- [22] J. Guillot, F. Fabreguette, L. Imhoff, O. Heintz, M.C. Marco de Lucas, M. Sacilotti, B. Domenichini, S. Bourgeois, Appl. Surf. Sci. 177 (2001) 268.
- [23] M. Shirkhanzadeh, Nanostruct. Mater. 5 (1995) 33.
- [24] U. Müller, R. Hauert, Thin Solid Films 290–292 (1996) 323.
- [25] G. Beamson, D. Briggs, High Resolution XPS of Organic Polymers: the Scienta ESCA300 Database, John Wiley and Sons, Chichester, 1992.
- [26] K.U. Klages, A. Wiltner, J. Luthin, Ch. Linsmeier, J. Nucl. Mater. 313–316 (2003) 56.
- [27] J.W. Robinson, CRC handbook of spectroscopy, CRC Press, Cleveland, Ohio, 1974–1981.
- [28] T.A. Carlson, Photoelectron and Auger spectroscopy, Plenum Press, New York NY, 1975.
- [29] J. Luthin, Ch. Linsmeier, Surf. Sci. 454–456 (2000) 78.
- [30] H. Bubert, X. Ai, S. Haiber, M. Heintze, V. Brüser, E. Pasch, W. Brandl, G. Marginean, Spectrochim. Acta, Part B: Atom. Spectrosc. 57 (2002) 1601.
- [31] M.-K. Seo, S.-J. Park, S.-K. Lee, J. Colloid Interface Sci. 285 (2005) 306.
- [32] T. Paulmier, J.M. Bell, P.M. Fredericks, Deposition of nano-crystalline graphite films by cathodic plasma electrolysis, submitted to Thin Solid Films.